Analytical Model for Injection-Controlled Excimer Laser Amplifiers

NAOYA HAMADA, ROLAND SAUERBREY, MEMBER, IEEE, AND FRANK K. TITTEL, FELLOW, IEEE

Abstract—**A semi-empirical model of a pulsed, injection-controlled laser is investigated analytically and is applied primarily to extensive experimental results that have been obtained for the XeF($C \rightarrow A$) excimer laser. The gain medium inside an unstable cavity is represented by a folded pulsed amplifier which is seeded by a narrow-band input signal. A set of coupled rate equations for the population densities of the upper laser states, the wide-band absorbers, and the photon flux was numerically integrated. Measured gain and absorption of the amplifier were used as input data to evaluate the model. Excellent agreement between calculated and experimentally observed peak intensity and various other pulse characteristics such as pulse shape and laser pulse delay time was obtained. This model also predicts the experimentally determined injection-control threshold for KrF excimer lasers successfully, and should be applicable to numerous other injection seeded lasers.**

I. INTRODUCTION

EXCIMER lasers can be efficiently tuned with a narrow spectral width using injection control and an unstable laser cavity [1], [2]. It is the purpose of this paper to develop a quantitative semi-empirical model that describes not only the characteristic behavior of such an injection-controlled excimer laser source, but also that of other similar laser systems. This requires a detailed analysis of the amplification process of a seed beam in an unstable laser cavity, where gain and absorption coefficients as well as the injection signal are functions of time.

Several analytical models have been developed for the laser amplification process. Homogeneously-broadened continuous wave (CW) lasers were analyzed by Rigrod [3], Schindler [4], and Eimerl [5]. Such models were successfully applied to relatively long pulse, high-gain lasers where a steady-state analysis is a good approximation. The temporal dependence of the gain as well as absorber saturation are generally neglected. For CW lasers, the mode characteristics in unstable resonators were investigated by Siegman *et al.* [6], [7]. Further work, including the analysis of pulsed laser oscillation in an unstable resonator, was reported by Isaev *et al.* [8], [9] and Ananev [10]. Kedmi and Treves [11] investigated injection locking of an unstable resonator for a CW laser, and Chow [12] studied the problem of line narrowing and frequency selection in an injection-locked laser. These treatments of injection control are particularly successful for high-gain CW lasers such as CO_2 lasers. However, they are unsuitable for the description of pulsed laser amplifiers where gain duration, photon lifetime in the unstable resonator, and the injected pulsewidth are on the same timescale. Laser pulse amplifiers with temporally-dependent gain coefficients were studied extensively by Icsevgi and Lamb [13], who described a full dynamic treatment of laser amplifiers ranging from the picosecond to the CW timescale, that included gain and absorber saturation effects. Similar work was published by Casperson [14]; however, in this case absorber saturation was not taken into account.

More specifically, KrF and XeF($B \rightarrow X$) excimer lasers with unstable resonators were simulated by Johnson *et al.* [15], [16]. An extensive kinetic model was reported that describes the temporal gain and absorber behavior of a long-pulse (500 ns–1 μs) excimer laser. By applying the model to the free-running oscillation process, excellent agreement was obtained with experiments; however, the injection-locking process was not analyzed in detail. Injection locking was investigated by several groups for pulsed TEA CO_2 lasers [17], [18], for pulsed dye lasers [19], [20], and for Q-switched YAG lasers [21], but loss saturation was not considered since these studies were concerned with media having a large gain–loss ratio. More recently, Voges and Marowsky [22] simulated the discharge-pumped injection-controlled XeF($C \rightarrow A$) laser system using a steady-state version of the relevant rate equations first given by Zhu *et al.* [23]. Bigio and Slatkine [1] presented a review of injection-locked, unstable resonator, excimer lasers. This work extensively discussed the experimental and qualitative aspects of injection control of high-gain KrF and XeF($B \rightarrow X$) excimer lasers, and provided a good starting point for the present analysis.

Despite this extensive body of work on laser amplifiers with and without injection control, there appears to be no analysis available that describes the behavior of a pulsed injection-controlled amplifier where such parameters as injected pulse width, gain duration, and photon lifetime in the unstable resonators are of arbitrary magnitude relative to each other. Therefore, a model was developed that is based on the dynamic behavior of laser amplifiers [13], coupled with some of the ideas on injection control of excimer lasers [1]. A rate equation approach is used, and the gain medium inside the unstable resonator is de-

Manuscript received May 16, 1988. This work was supported in part by the National Science Foundation, by the Office of Naval Research, and by the Robert Welch Foundation. The work of N. Hamada was supported in part by the Nippon Steel Corporation.

The authors are with the Department of Electrical and Computer Engineering, Rice University, Houston, TX 77251.

IEEE Log Number 8824023.

0018-9197/88/1200-2458$01.00 © 1988 IEEE

scribed as a folded amplifier seeded with an injected beam which expands due to the magnifying action of the unstable resonator and is simultaneously amplified [23]. This model is specifically applied to the injection-controlled XeF($C \rightarrow A$) laser [24]. The amplification process of this laser is characterized by the following features. 1) The line shape of the transition is homogeneously broadened as is the case for other excimer lasers. 2) The amplified linewidth of the output laser follows that of the injection-seed signal [2]. 3) The peak value of the small-signal gain is relatively low compared with that of other excimer lasers, due to the smaller stimulated emission cross section ($\sim 10^{-17}$ cm^2). Therefore, the laser performance strongly depends both on small-signal gain and absorption, and on their individual saturation behavior.

In order to investigate the amplification process, a model is required that can treat the transient behavior of photon flux, gain, and absorption, including the saturation of both gain and absorption. This type of analysis and its underlying physical assumptions are described in Section II. The validity of the model is also examined for the analytically solvable stationary case. Numerical results are compared with experiments in Section III, and the applicability of the model to predict the behavior of other injection-controlled systems is discussed. This model turns out to be sufficiently simple for easy implementation on personal computers.

II. Analytical Model

A. Model Description

Injection locking implies that the phase of the injected signal is controlled to match the mode structure of the amplifying laser [25]. None of the experiments concerning "injection locking" of excimer lasers that have been reported thus far [1], [2], [26] have made an attempt to control the temporal phase of the injected signal. The injected photons act rather as a seed signal within the homogeneously-broadened excimer transition, and force the laser to amplify the injected field. This leads to the control of laser linewidth, center wavelength for short gain duration (within the tuning range determined by the excimer transition), and beam divergence. Since no phase control is possible for these experiments, the expression *injection locking* is a misnomer—at least for excimer lasers. Injection seeding [1], [21], [25], or the more general term *injection control*, that would include locking as well as seeding should be used instead. Consequently, injection seeding can be considered by neglecting the phase of the laser field, i.e., in a rate equation approximation. If the linewidth of the injected signal is much smaller than the tuning range of the homogeneous laser transition, experiments show that the linewidth of the injection-controlled laser follows the injected linewidth for short pulse duration [1], [2]. Hence, the spectral intensity at the line center of the injected field is proportional to the spectrally-integrated intensity, which is also the experimentally simple-to-measure quantity that is usually used to characterize such lasers. Together with the homogeneous broadening of the laser transition, this implies that a wavelength-independent set of rate equations may be used for the spectrally-integrated laser photon flux q.

A rate equation description for a pulsed injection-controlled laser is therefore developed. The XeF($C \rightarrow A$) laser is used as a specific example; however, it is understood that most arguments hold equally well for many other pulsed laser systems. The effective gain of the XeF($C \rightarrow A$) laser is determined by the difference between the gain G and the absorption losses L. Due to the comparatively small stimulated emission cross section, the saturation intensity of the XeF($C \rightarrow A$) laser transition is higher than the saturation intensity for the dominant absorbers. Therefore, the laser photon flux can build up to a level where it saturates the absorbers before gain saturation occurs. Consequently, gain and absorption are saturable and have to be treated independently. It is also assumed that the transverse dimensions of the laser amplifier are much smaller than its longitudinal extent in the x direction, i.e., a one-dimensional analysis can be applied. Fig. 1 shows the traces of two rays at the edge of an injected laser beam introduced into a confocal unstable optical cavity of length d. The amplifying active medium of length l is indicated by dashed lines. In the unfolded resonator shown below, the beam expands exponentially due to the magnifying action of the resonator and is simultaneously amplified in the active medium. The expansion of the beam by itself leads to a decreasing intensity and can be treated like a distributed loss. Gain G, absorption loss L, and photon flux q in such an amplifier are related by the following set of rate equations [13], [23]:

$$\frac{\partial q(x,t)}{\partial x} + \frac{1}{v_g}\frac{\partial q(x,t)}{\partial t} = \frac{l}{d}G(x,t)q(x,t) - \frac{l}{d}L(x,t) \cdot q(x,t) - \frac{\ln(M)}{d}q(x,t) + \frac{N_C(t)}{\tau_{CA}}\frac{\Omega}{4\pi}\frac{\Delta\nu_I}{\Delta\nu_F} \quad (1)$$

$$\frac{\partial G(x,t)}{\partial t} = P_C(t)\sigma_{SE} - \frac{G(x,t)}{\tau_C} - G(x,t)\sigma_{SE}q(x,t) \quad (2)$$

$$\frac{\partial L(x,t)}{\partial t} = P_a(t)\sigma_a - \frac{L(x,t)}{\tau_a} - L(x,t)\sigma_a q(x,t) \quad (3)$$

where v_g is group velocity which is assumed to be constant and equal to the speed of light. M represents the unstable cavity magnification, $N_C(t)$ the population density of the XeF(C) states, i.e., the upper laser states, τ_{CA}, τ_C, and τ_a the radiative lifetime of the XeF($C \rightarrow A$) transition, the effective lifetime of the XeF(C) state, and the effective absorber lifetime, respectively; Ω is the relevant solid angle for the emission of spontaneous photons that contribute to the output signal, and $\Delta\nu_I$ and $\Delta\nu_F$ the line-

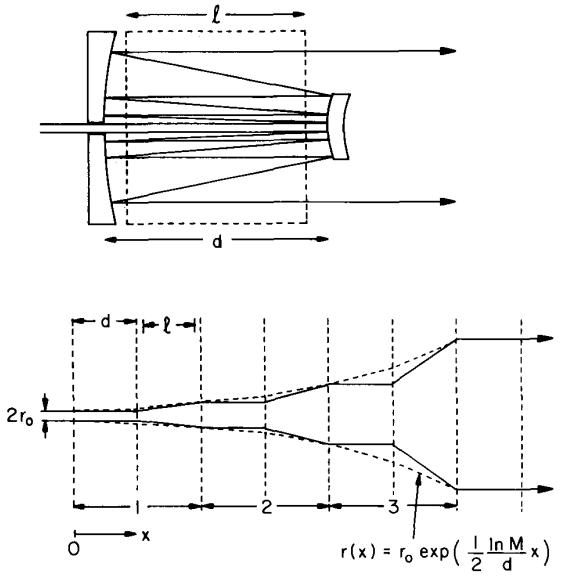

Fig. 1. Schematic representation of an injection-controlled unstable resonator and its unfolded amplifier model. The parameters d and l are the cavity length and the gain medium length, respectively. The dashed line in the bottom figure denotes the exponential beam expansion used in the model. r_0 describes the radius of the injection hole and $r(x)$ is the radius of the expanded beam after traveling the distance x in the unfolded amplifier.

widths of the injection source and the bandwidth of the laser transition, respectively. The production terms for the XeF(C) states and absorbers are denoted by $P_C(t)$ and $P_a(t)$, and σ_{SE} and σ_a are the stimulated emission and absorption cross sections.

On the right-hand side of (1), the first and second terms describe gain and loss. The third term is the photon flux loss per unit length due to the beam expansion inside the unstable cavity. The fourth term represents the contribution to the amplified signal due to spontaneous emission. On the RHS of (2) and (3), the first terms are the production terms. The second terms express the effective decay, and the third terms denote gain and loss saturation due to the photon flux in the cavity. The factor of l/d in (1) effectively distributes the active medium over the total cavity length d. This approximation is excellent when the factor l/d is sufficiently close to one ($0.6 \lesssim l/d \lesssim 1$). For smaller values of l/d, the region of the active medium and the unpumped region have been evaluated independently, and the results of such a calculation confirm the validity of the approximation.

The unsaturated gain data and loss shapes of $G_0(t)$ and $L_0(t)$ are obtained from experimental data [23]. The temporal profile of $G_0(t)$ is considered to be similar to that of the fluorescence signal of XeF($C \rightarrow A$) transition. The absolute peak value of $G_0(t)$ is set based on values suggested by kinetic modeling [27], [28]. $L_0(t)$ is obtained using $G_0(t)$ and the experimentally-obtained small-signal gain shape $[G_0(t) - L_0(t)]$. Although the net gain temporal profile of $[G_0(t) - L_0(t)]$ is strictly defined by the measured small-signal gain profile, the peak value of $G_0(t)$, and accordingly that of $L_0(t)$, may have an uncertainty of about ± 50 percent. It turns out that the maximum values for $G(t)$ and $L(t)$ can be chosen within these boundaries without changing the results of the calculation dramatically. The results depend primarily on the experimentally determined value of G–L, i.e., the net gain, as long as G and L individually are chosen in reasonable agreement with the overall boundaries of the specific laser system.

In a typical excimer laser, the production of the upper laser state and the relevant absorbers occurs in a complicated chain of kinetic reactions, and calculation of their effective production rates is difficult and cumbersome. On the other hand, when gain and absorption are determined as functions of time, either experimentally or by a kinetic code, they provide a measure of the number of excited states as functions of time which is determined by their respective production and decay processes. Therefore, once $G(t)$ and $L(t)$ are defined, the generally unknown production terms $P_C(t)$ and $P_a(t)$ may be obtained analytically from the unsaturated rate equations for $G_0(t)$ and $L_0(t)$ [(4) and (5) below], and used as inputs to the model.

$$P_C(t) = \frac{1}{\sigma_{SE}}\left[\frac{dG_0(t)}{dt} + \frac{G_0(t)}{\tau_C}\right] \tag{4}$$

$$P_a(t) = \frac{1}{\sigma_a}\left[\frac{dL_0(t)}{dt} + \frac{L_0(t)}{\tau_a}\right]. \tag{5}$$

The unstable cavity is treated like a folded amplifier, and additional gain or loss saturation due to double passing in the overlapping region of each photon flux path is neglected. This assumption is well justified if the magnification of the unstable resonator is sufficiently high ($M > 2$) because the overlapping volume of the double-passing photon flux becomes negligible under these conditions. However, in the case of small magnification values ($M < 1.3$), the overlapping volume approaches 50 percent of the one-pass total volume. With this assumption, the total amplifying gain length may be overestimated at most by a factor of two in the near saturated region. This effect causes saturation to occur slightly earlier than the experiments indicate because of the increase in injection power due to the above assumption. However, there should be no error associated with the unsaturated and totally saturated regions of the amplifer.

The injected laser flux is coupled into the rate equations by the initial condition for the photon flux $q(x, 0)$, which is given by

$$q(x, 0) = q(0, 0) \cdot \exp\left(-x\frac{\ln(M)}{d}\right) \tag{6}$$

where $q(0, 0)$ is the photon flux of the injection laser at the injection coupling hole (Fig. 1). The exponential function describes the expansion of the injected beam in the unstable resonator. This is a good approximation when the temporal change in the injected signal is slow compared to typical times that determine changes in the gain or loss. For short pulse injection, i.e., when the injected

signal changes on a time scale given by the transit time through the unstable resonator, the temporal evolution of the injected flux has also to be considered. Therefore, the injected photon flux at each location in the amplifier depends on the local time $t - x/v_p$ (see Appendix):

$$q(x, t) = q\left(0, t - \frac{x}{v_p}\right) \exp\left\{-x \frac{\ln(M)}{d}\right\}. \quad (7)$$

In order to compare the model results to a specific experiment, calculations were performed for the conditions of a recent series of experiments concerning the injection-controlled XeF($C \rightarrow A$) excimer laser [24]. The cavity length is $d = 12.5$ cm, the gain length is $l = 10$ cm, and the fractional solid angle of observation for the spontaneous emission term $\Omega/4\pi$ is $3 \cdot 10^{-5}$, which is determined by the fractional solid angle from the mid-point of the cavity to a 1.5 mm diameter injection-coupling hole. The ratio $\Delta\nu_I/\Delta\nu_F$ is $1.2 \cdot 10^{-2}$ and is given by the ratio of injection linewidth ($\Delta\nu_I = 0.6$ nm) to the bandwidth of the XeF($C \rightarrow A$) fluorescence spectrum ($\Delta\nu_F = 50$ nm). For the stimulated emission cross section, as well as for the relevant time constants, the following experimentally determined values were used:

$$\sigma_{SE} = 9.5 \cdot 10^{-18}\ \text{cm}^2\ [29], \quad \tau_C = 15\ \text{ns},$$

$$\tau_a = 20\ \text{ns}\ [28], \quad \text{and}\ \tau_{CA} = 100\ \text{ns}\ [30].$$

The role of absorbers is very important for the description of a XeF($C \rightarrow A$) amplifier because of its relatively small gain. From kinetic modeling and indirect experimental evidence [27], [28], [31], it may be concluded that highly-excited atomic xenon states and molecular ion species, such as Rg_2^+ and Rg_3^+ (with Rg being Ar, Kr, Xe), are the dominant absorbers for this laser. The photoionization cross-sections of the Xe*($5d$) and Xe*($6p$) states are approximately $2 \cdot 10^{-17}$ cm^2 in the blue-green [32], whereas the molecular ion photodissociation cross sections are about 10^{-18} cm^2 in the visible [33]. Since the relative abundance of these species is not precisely known, an approximate treatment of absorption was chosen for the purpose of this model. Instead of describing each absorbing species individually, an averaged absorber density associated with an averaged absorber cross section was used. Both numbers are, in principal, free parameters of the model. Their values, however, are strictly limited by several constraints. 1) The absorption coefficient, i.e., the density cross section product, is given by the value of the absorption coefficient in Fig. 2. 2) The absorber densities are limited by kinetic modeling to peak values on the order of $3 \cdot 10^{15}$ cm^{-3} to $1 \cdot 10^{16}$ cm^{-3} [28]. 3) The absorber cross section has to lie between the values determined by photoionization and those of photodissociation. A value of $\sigma_a = 3 \cdot 10^{-18}$ cm^2 was chosen, which is compatible with these boundary conditions.

Equations (1)–(3) have to be integrated numerically. The procedure is a variation of the predictor–corrector method outlined in [13]. Details of the numerical integration are given in the Appendix.

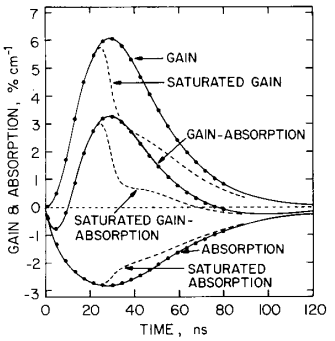

Fig. 2. Comparison of the gain and loss temporal shapes for the experimentally fitted gain–loss profiles (solid lines) and the integrated model results (dots) for the unsaturated region. For comparison, saturated temporal shapes are also indicated by dashed lines.

B. Model Verification

The following two approaches were adopted to establish the validity of the numerical integration model.

1) Gain Saturation for the Stationary Case: If gain and absorption are time independent and absorber saturation is neglected, then (1)–(3) may be simplified in the following way:

$$\frac{dq(x)}{dx} = \frac{l}{d} G(x)q(x) - \frac{l}{d} L(x)q(x) - \frac{\ln(M)}{d} q(x) + \frac{G(x)}{\tau_{CA}\sigma_{SE}} \frac{\Omega}{4\pi} \frac{\Delta\nu_I}{\Delta\nu_F} \quad (8)$$

$$G(x) = \frac{G(0)}{\left[1 + \dfrac{q(x)}{q_s}\right]} \quad (9)$$

$$L(x) = \text{const} \quad (10)$$

where $q_s = 1/(\sigma_{SE}\tau_C)$ is the saturation flux. This simplified set of equations describes a multipass amplifier where the beam expansion acts as an additional loss. For a sufficiently-strong injected signal $q(0)$, the fourth term of the RHS of (8) can be neglected. Then, (8) and (9) can be integrated analytically and yield

$$w(\gamma - \beta) = \ln\left[\frac{y}{y_0}\left(\frac{\beta y_0 - \gamma + \beta}{\beta y - \gamma + \beta}\right)^{\gamma/\beta}\right] \quad (11)$$

where $y = q(x)/q_s$ is the normalized photon flux, $y_0 = q(0)/q_s$ the normalized initial photon flux, $w = x/x_1$ the normalized traveling length, $\gamma = G(0)x_1$ the total unsaturated gain, $\beta = (L + (\ln(M)/d))x_1$ the total loss, and $x_1 = [2(\ln(R/r_0)/\ln(M)) + 1]d$ the total traveling length inside the cavity, where R denotes the outer radius of the output laser beam, and r_0 is the radius of the injection hole (Fig. 1). Equation (11) was evaluated using typical experimental parameters, and the analytical results were compared with those obtained by numerical integration as described in Section II-A for the same parameters. Since both calculations coincide with each other, the gain

saturation for the stationary case is treated correctly by the model.

2) Dynamic Behavior: The model uses the production terms of $P_C(t)$ and $P_a(t)$ as the inputs which are derived from $G_0(t)$ and $L_0(t)$. Then, the temporal profiles of gain and loss at each position are calculated by integrating (2) and (3). The model describes the dynamics of the unsaturated amplifier correctly if the calculated gain–loss profiles in the case of the unsaturated amplifier coincide with $G_0(t)$ and $L_0(t)$. Presented in Fig. 2 are the temporal profiles of $G_0(t)$, $L_0(t)$, and $G_0(t) - L_0(t)$. The solid lines correspond to the unsaturated gain and loss shapes which are derived according to the procedure described in Section II-A, while the points represent the model results at the output coupler for low-injection power, i.e., an unsaturated amplifier. The coincidence between both profiles confirms the correct treatment of the time-dependent, unsaturated injected amplifier.

III. Discussion

The model results are compared to experimental results obtained for the electron-beam pumped XeF($C \rightarrow A$) [24] and discharge pumped KrF($B \rightarrow X$) [1] lasers.

A. XeF($C \rightarrow A$) Laser

1) Input–Output Characteristics: Fig. 3 compares the calculated and measured laser output parameters as a function of power injected into an unstable resonator of magnification $M = 1.15$. In Fig. 3(a) the laser output energy is plotted as a function of injected laser power density which corresponds to the peak intensity of the dye laser injection source with a pulse duration of 250 ns (FWHM) [24]. The solid line corresponds to the calculated results, and the error bars represent experimental data. It should be noted that this figure compares absolute values and required no scale fitting or shifting. Except for the lowest output energy, excellent agreement is obtained. The slight difference between the model and experiment for the lowest output power is possibly due to the spatially-nonuniform pumping profile of the electron beam [24], which for this model is assumed to be uniform.

Fig. 3(b) and (c) show results for peak intensity and pulse duration (FWHM) as a function of injection power for the same experiments as in Fig. 3(a). The solid lines as above denote the calculated results and the error bars correspond to the experiments. The figures clearly demonstrate peak intensity saturation [Fig. 3(b)] and pulse shortening [Fig. 3(c)] with increasing injection power. Although the measured and calculated pulse durations agree within 10 percent, the calculated pulse duration is always slightly smaller than the experimental pulsewidth. There are two possible explanations for this result. 1) The temporal resolution of the diagnostic system is of the order of 1 ns; therefore, the real pulse duration might be slightly smaller than the measured one. 2) The measured unsaturated gain profile is averaged over the spatially-inhomogeneous pumping profile [24], which might impact on the output pulse duration.

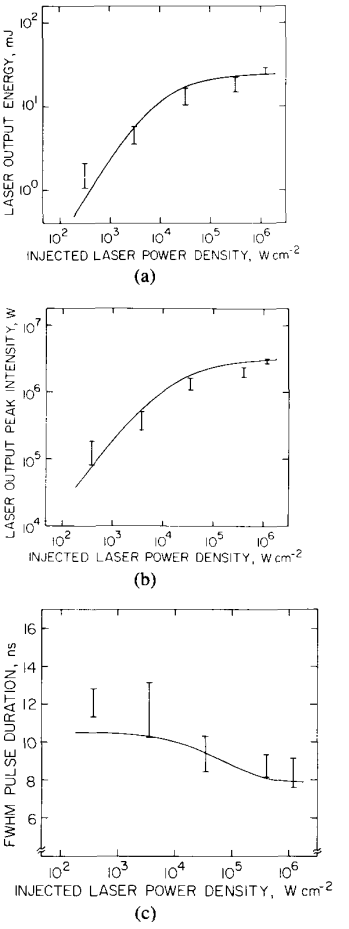

Fig. 3. Dependence of XeF($C \rightarrow A$) laser output energy (a), peak intensity (b), and pulse duration (FWHM) (c) on injection power density. The error bars are the experimental results for cavity magnification of $M = 1.15$, and the solid lines depict the corresponding model results.

2) Temporal Behavior: The temporal pulse shape of the laser output is compared to the calculated waveform for a typical experiment in Fig. 4. The experimental conditions corresponded to an injection power of 1.2 MW/cm^2 and an output energy of 25 mJ, which occurs in the saturated region of the amplifier [see Fig. 3(a)]. The solid line is the observed profile, while the dashed line represents the calculated pulse. For comparison, the dotted line shows the electron-beam pump pulse. The measured and analyzed profiles agree remarkably well in peak intensity, pulse duration, asymmetric pulse shape, and pulse position. In fact, none of the parameters representing the horizontal and vertical scales, including the relative timing of the pulses, was fitted. The calculated temporal behavior of gain and absorption are shown in Fig. 2. Gain and absorption saturation are apparent for high injected signals and high output power densities.

An increased injected signal leads to a more rapid buildup of the amplified pulse. This causes the output peak

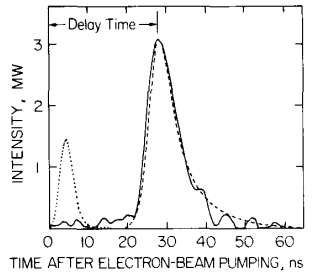

Fig. 4. A temporal profile comparison of XeF($C \rightarrow A$) laser output at 1.2 MW/cm^2 injection power density. The solid line is the observed profile, while the dashed line represents the model output, and the dotted line shows the electron-beam excitation pulse.

position to move toward earlier times relative to the pumping pulse. The time delay between the maximum of the output pulse and the beginning of the pumping pulse (Fig. 4) is shown in Fig. 5. The solid line is calculated and the error bars correspond to the measured values. It should be noted again that the calculated and the experimental values are in excellent agreement. The error is less than 3 ns, which is comparable to the experimental reproducibility considering the temporal resolution of the measuring system and effects of the instrumentation noise.

3) Laser Output Energy Dependence on Cavity Magnification: Experiments were conducted for various cavity magnification values of M = 1.05, 1.08, 1.15, and 1.23 [24]. For the evaluation of cavity magnification effects on laser output, the beam divergence of the injected seed beam has to be taken into account, which depends upon the original divergence from the injection source (1–1.5 mrad) and on diffraction effects at the injection hole (Fig. 1). For small cavity magnifications, the divergence becomes comparable or greater than the beam expansion factor due to the unstable cavity magnification. This results in higher values of the equivalent magnification values than those calculated by a simple parallel beam approximation for the injected signal and, consequently, in shorter transit times inside the amplifier [22]. This corresponds to a shortening of the amplification length in the folded amplifier model. Based on the injection laser beam divergence and the focusing optics for the injection source, a typical beam divergence of 1.4 mrad inside the cavity was obtained, and the corrected magnification values were derived by ray-tracing methods. As mentioned above, the beam divergence of the injection beam impacts only on the two smaller magnification values, i.e., M = 1.05 and 1.08. Thus, the equivalent magnification values become M = 1.10, 1.13, 1.15, and 1.23 instead of M = 1.05, 1.08, 1.15, and 1.23, respectively. The laser output was calculated using these values and the results were compared to experiments in Fig. 6 for injection power densities of (a) 1.2 MW/cm^2 (saturated region) and (b) 3.5 kW/cm^2 (small-signal amplification). The solid and dotted lines are the calculated results, and the solid and dotted error bars represent the experiments for the two different injection power density values, respectively. The

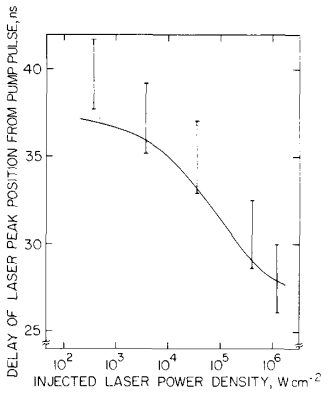

Fig. 5. Dependence of laser output pulse peak position on injection power density. The error bars are the experimental results for cavity magnification of M = 1.15, and the solid line represents the corresponding model output.

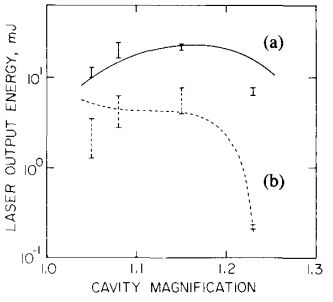

Fig. 6. Dependence of the amplified laser output energy on cavity magnification. The solid and dotted lines are the model outputs for injection power density values of (a) 1.2 MW/cm^2 and (b) 3.5 kW/cm^2, respectively. The solid and dotted error bars show the corresponding experimental results.

agreement between measured and calculated values is reasonable, considering that again no parameter fitting was employed. In fact, the optimum magnification and the overall dependence of the laser output on the magnification are calculated correctly. The disagreement at M = 1.23 for high injected power density is probably due to partially spatial saturation of the gain at the center of the pumping region because of the spatially nonuniform pumping profile which is not considered in the model. On the other hand, the disagreement at M = 1.05 for low injected power density is possibly due to the breakdown of the geometrical optics approximation for these conditions. However, in the saturated regime, good agreement between experiments and the calculation is obtained for small magnifications (M = 1.05). This is to be expected because of the insensitivity of the energy output on the amplifier length for the saturated laser.

4) Laser Output Energy Dependence on Pumping Power: The dependence of the amplifier gain on electron beam pumping power was investigated experimentally [24]. Using the measured peak gain value, the model was applied to estimate the dependence of the amplifier output on the pumping power for a cavity magnification of M =

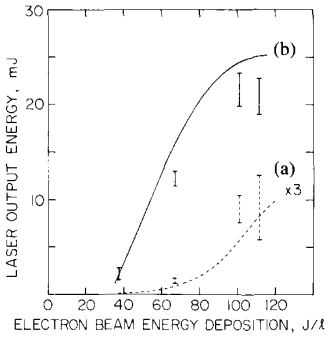

Fig. 7. Laser output energy dependence on the electron-beam pumping power for a cavity magnification of $M = 1.15$. The dotted and solid lines are the model outputs for injection power density values of (a) 400 W/cm^2 and (b) 370 kW/cm^2, respectively. The dotted and solid error bars represent the corresponding experimental data.

1.15. The temporal profiles of $G_0(t)$ and $L_0(t)$ for different pumping conditions are assumed to have similar shapes; only the peak values depend on the pumping power input. This is confirmed by experiments. Fig. 7 shows the model calculations together with the experimental data for injection power densities of (a) 400 W/cm^2 and (b) 370 kW/cm^2. Experimental data show an exponential relationship between pumping power and laser output energy for lower injected powers and the consequently low output signals [Fig. 7(a)]. It becomes linear and then saturates for large injection powers [Fig. 7(b)]. From Fig. 7, it is evident that the model predicts this behavior quite well. Furthermore, the calculated results predict the output energy of the injection-controlled amplifier with considerable accuracy.

B. KrF Laser

Thus far, the model has been applied to the injection-controlled XeF($C \rightarrow A$) excimer laser amplifier; however, it is not necessary to restrict its application to this specific system. Since the model can handle the transient behavior of the photon flux as well as the saturation of gain and loss, it can be applied to other kinds of homogeneously-broadened, injection-controlled lasers, such as other excimer, dye, and CO_2 lasers.

In order to investigate the applicability of the model to lasers other than the XeF($C \rightarrow A$) system, typical excimer laser conditions were selected, and the injection-control threshold was evaluated for various combinations of small-signal gain values and injection intensity levels. The temporal profiles of $G_0(t)$ and $L_0(t)$ are assumed to have similar shapes to those shown in Fig. 2, but the peak value of the absorption losses $L_0(t)$ is fixed to be 0.01 cm^{-1}. The peak value of the gain $G_0(t)$ is then altered to realize different small-signal net gain values. Cross sections for stimulated emission and absorption are assumed to be 2×10^{-16} and 2×10^{-17} cm^2, respectively. The radiative lifetime of the upper state is set to be 10 ns, and the effective lifetimes of the upper state and the absorbers are both assumed to be 2 ns. This corresponds to typical conditions in a discharge-pumped KrF excimer laser. For

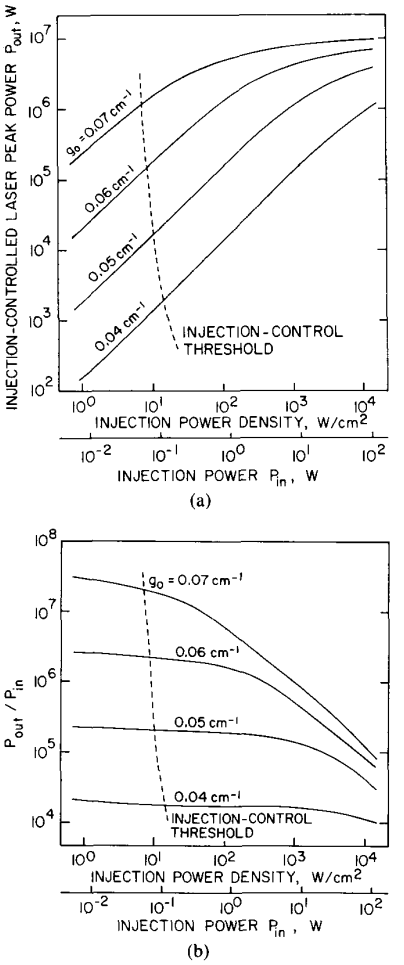

Fig. 8. Calculated results for typical KrF excimer laser conditions: (a) amplified laser output (P_{out}) versus injection power density; (b) output-input power ratio versus injection power density. For comparison, injection powers into a 1 mm diameter injection hole (P_{in}) are shown in both (a) and (b). (g_0: peak value of small signal net gain, magnification $M = 4.0$, cavity length $d = 62.5$, gain medium length $l = 62.5$ cm, stimulated emission cross section $\sigma_{SE} = 2 \times 10^{-16}$ cm^2, absorber cross section $\sigma_a = 2 \times 10^{-17}$ cm^2, radiative lifetime of the upper state = 10 ns, effective lifetimes of the upper state and the absorbers = 2 ns, outer diameter of output laser beam = 16 mm.)

those conditions the laser saturation intensity is considerably lower than the absorber saturation intensity. Therefore, absorber saturation for the KrF($B \rightarrow X$) laser is less important than for the XeF($C \rightarrow A$) laser. Cavity magnification M was chosen to be 4.0, and the cavity length d and gain medium length l are 62.5 cm. The injection hole diameter is 1 mm, and the outer diameter of output laser beam is set to be 16 mm. These conditions correspond closely to those of the experiments reported by Bigio and Slatkine [1]. The injection-control threshold was evaluated by comparing the peak power of the amplifier laser output within the narrow linewidth of the injected signal and that of the free-running laser within the wide bandwidth which builds up from spontaneous emission.

Fig. 8(a) shows the injection-controlled laser peak

power P_{out} as a function of injection power density for four different small-signal peak gain values g_0. For comparison, the absolute value of injection power at a 1 mm diameter injection hole (P_{in}) is shown in the bottom of the figure. The dotted line in the figure represents the injection-control threshold which is defined as the injected power density that causes a narrow-band injection-controlled output equal to the free-running power density. The output powers in the saturated region are on the order of several MW cm^{-2} for a gain of 6–7 percent cm^{-1}, which is typical for free-running, as well as injection-controlled excimer lasers. The injection threshold of ~ 0.1 W injected power into a 1 mm diameter injection hole is in excellent agreement with experiments [1]. Further investigation of the model suggests that efficient injection-control cannot be achieved if the small signal gain value exceeds $g_0 \approx 0.08\ cm^{-1}$ for the given geometric conditions. When the laser is a pure ASE laser that can be driven to saturation in one pass, only injection-control of the amplification process close to the optical axis has a negligible effect on the quality of the laser output. Presented in Fig. 8(b) is the output–input power ratio (P_{out}/P_{in}) as a function of injection power density for the same conditions as those shown in Fig. 8(a). An output power–input power ratio of $\sim 10^6$ was obtained for a typical discharge-pumped KrF laser ($g_0 = 0.05$–$0.06\ cm^{-1}$), showing good agreement with experiments reported in [1].

Appendix
Numerical Integration Procedure

In order to integrate (1)–(3), it is desirable to eliminate the second term on the left-hand side of (1). For this purpose, it is possible to use the local time τ as opposed to the global time t by introducing $\tau = t - x/v_g$ as in [13], [14]. However, for the case of quasi-CW dye laser injection [24], this method cannot be applied since the amplified output could appear even at negative local times. The reason for this is that the whole amplifier is filled with seed photons when the gain becomes positive for the quasi-CW injection case; therefore, the amplified output experiences a gain length which is less than the total transit length inside the cavity, and could appear at negative local times.

In order to overcome this problem, the global time can be used. If the temporal integration step on the global time axis coincides with the transit time delay of the photons for one spatial integration step, this integral is equivalent to that along the same local time axis. Although this approach does not allow for a free setting of the temporal and spatial integration steps, it permits elimination of the second term on the LHS of (1) and avoids negative local times. Consequently, the spatial integration of $q(x, t)$ is conducted without introducing the local time parameter in the following way:

$$q(x + 2H_s, t + 2\Delta t) = q(x, t) + 2H_s \frac{\partial q(x + H_s, t + \Delta t)}{\partial x}. \quad \text{(A1)}$$

Here Δt is a time step of the integration, and H_s is a spatial step which is given by $H_s = v_g \Delta t$; i.e., 12.5 cm in the model. Since this approach treats the global time, not only the quasi-CW injection but also the short pulse injection case can be analyzed by this method. For the latter, it is equivalent to a local time treatment [equation (7)].

The numerical integration procedure is based on the predictor–corrector method [13]. If y denotes $q(x, t)$, $G(x, t)$, or $L(x, t)$, and y' denotes $\partial q(x, t)/\partial x$, $\partial G(x, t)/\partial t$, or $\partial L(x, t)/\partial t$, the predictor procedure is expressed by

$$y_2 = y_0 + 2\Delta y_1' \quad \text{(A2)}$$

where Δ is an integration step, and the suffix represents the spatial or temporal position. Next, y_2' is derived using the result of the former predictor. Then, the value of y_2 is corrected by (A3).

$$y_2 = y_1 + 0.5\,\Delta(y_1' + y_2'). \quad \text{(A3)}$$

For the first step of the integration, y_{-1} is not given; accordingly, predictor [$y_1 = y_0 + \Delta y_0'$], derivation of y_1', and corrector [$y_1 = y_0 + 0.5\,\Delta(y_0' + y_1')$] procedures are iterated until the value of correction becomes sufficiently small. These procedures are applied to (1)–(3) both in the temporal and spatial domains.

Acknowledgment

The authors would like to acknowledge valuable suggestions and a critical review of the manuscript by I. J. Bigio and W. L. Nighan.

References

[1] I. J. Bigio and M. Slatkine, "Injection-locking unstable resonator excimer lasers," *IEEE J. Quantum Electron.*, vol. QE-19, pp. 1426–1436, 1983; also in *Opt. Lett.*, vol. 7, pp. 19–21, 1982.

[2] F. K. Tittel, G. Marowsky, W. L. Nighan, Y. Zhu, R. A. Sauerbrey, and W. L. Wilson, Jr., "Injection-controlled tuning of an electron beam excited XeF($C \rightarrow A$) Laser," *IEEE J. Quantum Electron.*, vol. QE-22, pp. 2168–2173, 1986.

[3] W. W. Rigrod, "Homogenerously broadened CW lasers with uniform distributed loss," *IEEE J. Quantum Electron.*, vol. QE-14, pp. 377–381, 1978.

[4] G. M. Schindler, "Optimum output efficiency of homogeneously broadened lasers with constant loss," *IEEE J. Quantum Electron.*, vol. QE-16, pp. 546–550, 1980.

[5] D. Eimerl, "Optical extraction characteristics of homogeneously broadened CW lasers with nonsaturating lasers," *J. Appl. Phys.*, vol. 51, pp. 3008–3016, 1980.

[6] A. E. Siegman and H. Y. Miller, "Unstable optical resonator loss calculations using the Prony method," *Appl. Opt.*, vol. 9, pp. 2729–2736, 1970.

[7] E. A. Sziklas and A. E. Siegman, "Mode calculations in unstable resonators with flowing saturable gain—II: Fast Fourier transform method," *Appl. Opt.*, vol. 14, pp. 1874–1889, 1975.

[8] A. A. Isaev, M. A. Kazaryan, G. G. Petrash, S. G. Rautian, and A. M. Shalagin, "Evolution of Gaussian beams and pulse stimulated emission from lasers with unstable resonators," *Sov. J. Quantum Electron.*, vol. 5, pp. 607–614, 1975.

[9] ——, "Shaping of the output beam in a pulsed gas laser with an unstable resonator," *Sov. J. Quantum Electron.*, vol. 7, pp. 746–752, 1977.

[10] Y. A. Anańev, "Establishment of oscillations in unstable resonators," *Sov. J. Quantum Electron.*, vol. 5, pp. 615–617, 1975.

[11] J. Kedmi and D. Treves, "Injection-locking optimization in unstable resonators," *Appl. Opt.*, vol. 20, pp. 2108–2112, 1981.

[12] W. W. Chow, "Theory of line narrowing and frequency selection in

an injection locked laser," *IEEE J. Quantum Electron.*, vol. QE-19, p. 243, 1983.
[13] A. Icsevgi and W. E. Lamb, Jr., "Propagation of light pulses in a laser amplifier," *Phys. Rev.*, vol. 185, pp. 517-545, 1969.
[14] L. W. Casperson, "Analytic modeling of gain-switched lasers—II: Laser amplifiers," *J. Appl. Phys.*, vol. 47, pp. 4563-4571, 1976.
[15] T. F. Johnson, Jr., L. J. Palumbo, and A. M. Hunter, II. "Kinetics simulation of high-power gas lasers," *IEEE J. Quantum Electron.*, vol. QE-15, pp. 289-301, 1979.
[16] T. F. Johnson, Jr. and A. M. Hunter, II, "Physics of the krypton fluoride laser," *J. Appl. Phys.*, vol. 51, pp. 2406-2420, 1980.
[17] D. M. Tratt, A. K. Kar, and R. G. Harrison, "Spectral control of gain-switched lasers by injection-seeding: Application to TEA CO_2 systems," *Prog. Quantum Electron.*, vol. 10, pp. 229-266, 1985.
[18] H. Tashiro, T. Shimada, K. Toyoda, and S. Hamba, "Studies on injection locking of a TEA-CO_2 laser for stable high-power operation," *IEEE J. Quantum Electron.*, vol. QE-20, pp. 159-165, 1984.
[19] U. Ganiel, A. Hardy, and D. Treves, "Analysis of injection locking in pulsed dye laser systems," *IEEE J. Quantum Electron.*, vol. QE-12, pp. 704-716, 1976.
[20] P. Flamant and G. Mégie, "Frequency locking by injection in dye lasers: Analysis of the CW and delta pulse regimes," *IEEE J. Quantum Electron.*, vol. QE-16, pp. 653-660, 1980.
[21] J-Y. Park, G. Guiliani, and R. L. Byer, "Single axial mode operation of a Q-switched Nd:YAG oscillator by injection seeding," *IEEE J. Quantum Electron.*, vol. QE-20, pp. 117-125, 1984.
[22] H. Voges and G. Marowsky, "Injection control of a discharge excited XeF($C \rightarrow A$) laser," *IEEE J. Quantum Electron.*, vol. 24, pp. 827-832, 1988.
[23] Y. Zhu, R. Sauerbrey, F. K. Tittel, and W. L. Wilson, Jr., "Injection controlled operation of a broadband excimer laser," in *Proc. 2nd Int. Laser Sci. Conf., AIP Conf. Proc.*, no. 160, pp. 30-32, 1987.
[24] N. Hamada, R. Sauerbrey, W. L. Wilson, Jr., F. K. Tittel, and W. L. Nighan, "Performance characteristics of an injection-controlled electron-beam pumped XeF($C \rightarrow A$) laser system," *IEEE J. Quantum Electron.*, vol. 24, pp. 1571-1578, 1988.
[25] A. E. Siegman, *Lasers*. Mill Valley, CA: University Science, 1986, p. 1129-1170.
[26] J. B. West, H. Komine, and E. A. Stappaerts, "Efficient injection-locking of an E-beam-excited XeF laser," *J. Appl. Phys.*, vol. 52, pp. 5383-5385, 1981.
[27] W. L. Nighan, R. Sauerbrey, Y. Zhu, F. K. Tittel, and W. L. Wilson, Jr., "Kinetically-tailored properties of electron beam excited XeF($C \rightarrow A$) and XeF($B \rightarrow X$) laser media using an Ar-Kr buffer mixture," *IEEE J. Quantum Electron.*, vol. QE-23, pp. 253-261, 1987.
[28] W. L. Nighan and M. C. Fowler, "Kinetic processes in XeF($C \rightarrow A$) laser media excited by a high current density electron beam," *IEEE J. Quantum Electron.*, submitted for publication.
[29] W. K. Bischel, D. J. Eckstrom, H. C. Walker, Jr., and R. A. Tilton. Photolytically pumped XeF($C \rightarrow A$) laser studies," *J. Appl. Phys.*, vol. 52, pp. 4429-4434, 1981.
[30] R. Sauerbrey, W. Walter, F. K. Tittel, and W. L. Wilson, Jr., "Kinetic processes of electron beam generated XeF* and Xe_2F* excimers," *J. Chem. Phys.*, vol. 78, pp. 735-747, 1983.
[31] Y. Nachshon, F. K. Tittel, W. L. Wilson, Jr., and W. L. Nighan "Efficient XeF($C \rightarrow A$) laser oscillation using electron-beam excitation," *J. Appl. Phys.*, vol. 56, pp. 36-45, 1984.
[32] C. Duzy and H. A. Hyman, "Photoionization of excited rare-gas atoms," *Phys. Rev. A.*, vol. 22, no. 5, pp. 1878-1883, 1980.
[33] D. B. Geohegan and J. G. Eden, "Xe_2Cl and Kr_2F Excited State ($4^2\Gamma$) absorption spectra: Measurements of absolute cross sections," *Chem. Phys. Lett.*, vol. 139, pp. 519-524, 1987.

Naoya Hamada, for a photograph and biography, see p. 1578 of the August 1988 issue of this JOURNAL.

Roland Sauerbrey (M'85), for a photograph and biography, see p. 1578 of the August 1988 issue of this JOURNAL.

Frank K. Tittel (SM'72-F'86), for a photograph and biography, see p. 1578 of the August 1988 of this JOURNAL.